Optical Transition Radiation

Beth Gitter*
UCLA Department of Physics
Center For Advanced Accelerators
Particle Beam Physics Lab
Los Angeles, CA 90024

Abstract

The use of Optical Transition Radiation (OTR) as an on-line diagnostic system for the UCLA Particle Beam Physics Lab electron beam has been investigated. Beam divergence, energy and profile are some of the properties which have been theoretically and experimentally (past works) shown to be analyzable and measurable from OTR patterns. Calculations regarding the survivability of both the beam and the OTR target are made for various beam energies and target materials. It is found that a 20 MeV beam passing through a thin aluminum target will be unperturbed, in terms of energy and angular divergence, and the target will not be destroyed. Finally, the use of an OTR double-foil interferometer, as a more precise diagnostic tool, is presented for future consideration.

*Work supported by UCLA Physics department

Contents

Introduction

A low-emittance, high-brightness electron beam is being constructed at the UCLA Center for Advanced Accelerators (CAA), a Particle Beam Physics Lab (PBPL). The beam will be used to drive a Free-Electron LASER[1] and a Plasma Wake-Field Accelerator (PWFA)[2]. The laser-driven photo-cathode RF electron gun is expected to produce a 4.5 MeV beam, which when directed through a Plane-Wave Transformer (PWT) linac[3] will achieve energies of about 20 MeV.

It is desired to implement a diagnostic tool to determine the characteristics of the beam before (4.5 MeV) and after (20 MeV) linac. A charge collecting phosphor screen monitored by a CCD camera has been employed for beam observation. However, due to its integrating nature, in addition to registering the charge of the photo-electron bunch, the phosphor also collects the undesirable dark current which can exceed the photo-electrons.

Another possible diagnostic system is Cerenkov radiation (produced when a charge passes through a medium at velocities greater than the phase velocity of light in that medium) emitted from a target material such as quartz. Typically the light produced in this process is emitted at angles around 45° with respect to the beam axis. Such radiation can be difficult to image (via video) because of limited admittance and inherent divergence[4].

This paper presents a study of the characteristics of Transition Radiation (TR), with emphasis on use with the UCLA electron beam. Transition Radiation has a broad spectrum which can extend from microwave to x-ray frequencies with substantial intensities. For electron beam monitoring we would like to exploit the optical (visible) portion of the electromagnetic spectrum since cameras and other optical equipment are readily available at these wavelengths. With appropriate implementation of the device, Optical Transition Radiation can provide an on-line (non-destructive) diagnostic tool that gives information

about the beam's profile, energy and divergence. The theoretical background will be developed, and the parameters relevant to both the 4.5 MeV and 20 MeV beams will be considered for quantitative experimental analysis.

Theory

Transition Radiation In General

The existence of transition radiation was theoretically predicted by Frank and Ginzburg in 1946[5]. The effect can be understood by considering the electromagnetic fields that a moving charged particle carries with it. These fields are media dependent on the dielectric constant ϵ. As a moving charge approaches and crosses the boundary between two different media the fields must somehow reorganize themselves. It is in this process of reorganization that some of the fields are "shaken off" as transition radiation.

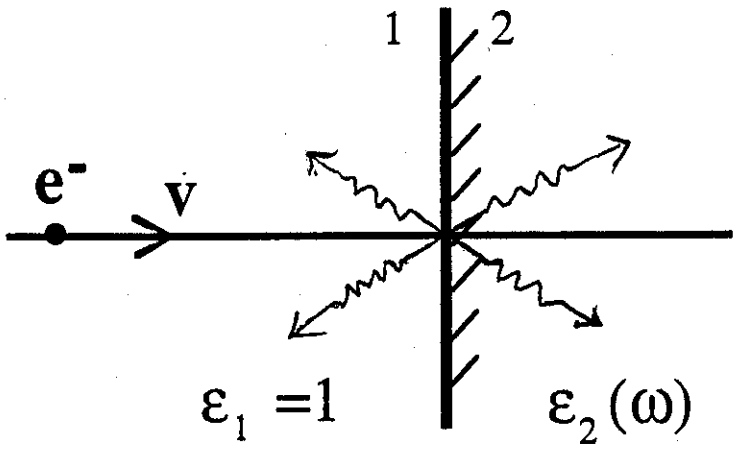

Figure 1. Photons are generated in both forward and backward directions. The radiation propagates away from the boundary into both media.

The radiation pattern produced by a beam of electrons

traversing a boundary can be analyzed to yield information about the beam.

The angular distribution of the radiation can be understood by a "phase coherence" argument given by Jackson[6]. The driving fields of the incident particle penetrate into medium 2 as the particle approaches the boundary (see figure 1). For appreciable radiation to be emitted there must be coherent superposition of the fields (particle fields and radiation fields) from different points in the medium. This will occur provided that the product of the driving fields of the particle and the generated wave does not experience a significant change in phase over the region of medium 2. This results in the condition for appreciable transition radiation to occur when medium 1 is vacuum:

$$\sqrt{\epsilon(\omega)}\ \gamma\theta \leq 1 \qquad (1)$$

where γ is the Lorentz factor, θ is the angle of radiation emission with respect to the beam axis, ϵ is the dielectric constant of medium 2, and ω is the radiation frequency. The characteristic angular distribution for the emission of transition radiation is that of a narrow cone with apex angle $\theta \sim 1/\gamma$.

The general approach to finding a relation for the intensity of TR involves using Maxwell's equations to solve for the radiation fields in the two media, applying the necessary boundary conditions, and calculating the intensity of the emitted radiation. The most general result for the case of an electron passing from medium 1 (with dielectric constant ϵ_1) into medium 2 (with dielectric constant ϵ_2) at normal incidence to the boundary is presented (equation 2) by Ter-Mikaelian[7]. Similar results are derived by Ginzburg and Tsytovich[8] and Pafomov[9]. The spectral intensity, I, of the radiation emitted forward (into

medium 2) in the frequency range dω and into a solid angle dΩ is given by:

$$\frac{d^2I_2(\theta,\omega)}{d\omega\, d\Omega} = \frac{e^2\beta^2\sqrt{\epsilon_2}\sin^2\theta_2\cos^2\theta_2}{\pi^2 c} \times \left| \frac{(\epsilon_1 - \epsilon_2)(1 - \beta^2\epsilon_2 - \beta\sqrt{\epsilon_1 - \epsilon_2\sin^2\theta_2})}{(1 - \beta^2\epsilon_2\cos^2\theta_2)(1 - \beta\sqrt{\epsilon_1 - \epsilon_2\sin^2\theta_2})(\epsilon_1\cos\theta_2 + \sqrt{\epsilon_1\epsilon_2 - \epsilon_2^2\sin^2\theta_2})} \right|^2 \quad (2)$$

where θ_2 is the angle between the forward T.R. wave-vector and the beam axis, β is the normalized electron velocity, e is the charge on the electron, and ω is the frequency of radiation. The radiation propagating in the backward direction is given by the same equation with the permutation of subscripts $1 \rightarrow 2$ and $\beta \rightarrow -\beta$. The dependence on the parameters included in equation (2) will be determined in a specific instance by the values $\epsilon_1(\omega)$ and $\epsilon_2(\omega)$. It is necessary, therefore, to understand something about dispersion in materials.

Model of Dispersion[10]

The atomic contribution to the dielectric constant of a material in the presence of an external electric field, **E**, is given by:

$$\epsilon(\omega) = 1 + 4\pi\chi_e = 1 + 4\pi\frac{\vec{P}}{\vec{E}} \quad (3)$$

where χ_e is the electric susceptibility and **P** is the macroscopic polarization. The dipole moment contributed by a single electron is $p_j = -ex_j$, so we need to determine the displacement x_j. The equation of motion for an electron bound to an atom of the material by a harmonic force and acted on by an electric field **E** is written as

$$m\,[\,\ddot{x}_j + \Gamma_j \dot{x}_j + \omega_j^2 x_j\,] = -e\vec{E} \qquad (4)$$

where ω_j is the binding frequency, and Γ_j (typically $<< \omega_j$) is a measure of the damping force. For a molecular density N with Z electrons per molecule, and taking into account the different oscillator strengths f_j ($\Sigma f_j = Z$) that correspond to ω_j and Γ_j, the macroscopic polarization is a sum of the contributions from individual electrons: $\mathbf{P} = N\,\Sigma(f_j p_j)$. The dielectric constant is now of the form:

$$\epsilon(\omega) = 1 + \frac{4\pi N e^2}{m} \sum_j f_j\,(\omega_j^2 - \omega^2 - i\omega\Gamma_j)^{-1}\,. \qquad (5)$$

Note that binding frequencies in atoms must be of the order of light frequencies, and as stated earlier the spectrum of T.R. can extend beyond optical frequencies into the x-ray region.

Consider now the high frequency limit, where ω is far above the highest binding frequency ω_j. The terms ω_j^2 and $i\omega\Gamma_j$ in the denominator of equation (5) become very small compared to ω^2 and the dielectric constant simplifies to a plasma formula:

$$\epsilon(\omega) \approx 1 - \frac{\omega_p^2}{\omega^2} \qquad \text{where } \omega_p^2 = \frac{4\pi NZe^2}{m} \qquad (6)$$

In dielectric media, equation (6) only applies for $\omega^2 >> \omega_p^2$, and $\epsilon(\omega)$ is then close to unity, but slightly less. An exception to this constraint occurs in situations like that of a tenuous electron plasma, wherein the electrons are free ($\omega_j = 0$) and the damping is negligible. Then equation (6) holds even for frequencies $\omega < \omega_p$. The radiation wave number is given by

$$k = \frac{1}{c}\sqrt{\omega^2 - \omega_p^2} \qquad (7)$$

For $\omega < \omega_p$ k is purely imaginary and the fields inside the medium (plasma) fall off exponentially from the boundary. Such waves incident on the plasma are almost entirely reflected from

the surface.

In metals there are free electrons, and at optical frequencies the response of these free electrons to an external field dominates dispersion. This constitutes a situation like that of the plasma described above which is why metals appear shiny in light. Optical frequencies are of the order 10^{15} Hz, and for most metals the plasma frequency is on the order of 10^{16} Hz. For optical frequencies in metals the dielectric constant is large and negative:

$$\epsilon \approx 1 - (10^{16}/10^{15})^2 \sim -100$$

Radiation at optical frequencies does not penetrate far into a metal from the boundary. When the complex wave number is written in the form $k = \beta + i\alpha/2$, the attenuation constant is given by the parameter α. The attenuation length, $1/\alpha$, is in this case

$$\frac{1}{\alpha} \approx \frac{c}{2\sqrt{\omega_p^2 - \omega^2}} \sim 0.015\ \mu m \qquad (8)$$

For a metal foil of thickness larger than α^{-1} the OTR produced by an electron beam, passing from vacuum into the foil and emerging again in vacuum, will be primarily emitted into the vacuum. Further explanation as to why it is desirable to use a metal boundary to attain this situation will be given, but first the spectral intensity of OTR in such a case is analyzed.

<u>OTR In Metals, Relativistic Limit</u>

As the charge moves from the medium ($\epsilon_1 = \epsilon$) into vacuum ($\epsilon_2 = 1$), the radiation emitted forward is given by equation (2):

$$\frac{d^2I_2}{d\omega d\Omega} = \frac{e^2\beta^2}{\pi^2 c} \frac{\sin^2\theta \cos^2\theta}{(1-\beta^2\cos^2\theta)^2} \times \left| \frac{(\epsilon-1)\,(1-\beta^2-\beta\sqrt{\epsilon-\sin^2\theta})}{(\epsilon\cos\theta+\sqrt{\epsilon-\sin^2\theta})\,(1-\beta\sqrt{\epsilon-\sin^2\theta})} \right|^2 \qquad (9)$$

For relativistic electrons $\beta \to 1$, and in the case where $|\epsilon| > 1$, the third term in (9) tends to unity. (This is most easily seen by noting that from equation (1) $\theta << 1$, so one can use the approximations: $\sin^2\theta \approx 0$, $\cos\theta \approx 1$.) A simplification of the remaining terms is made obvious by the substitution $x = \beta\cos\theta$ (note $x \approx 1$)

$$\frac{x^2}{(1 - x^2)^2} = \frac{1}{(1 + \frac{1}{x})^2 (1 - x)^2} \approx \frac{1}{4 (1 - x)^2} \qquad (10)$$

Equation (9) takes the form:

$$\frac{d^2 I_2}{d\omega d\Omega} = \frac{e^2}{4\pi^2 c} \frac{\sin^2\theta}{(1 - \beta\cos\theta)^2} \approx \frac{e^2}{\pi^2 c} \frac{\theta^2}{[\theta^2 + \gamma^{-2}]^2} \qquad (11)$$

where the small angle approximations and $\beta \approx 1 - 1/(2\gamma^2)$ have been used to obtain the form on the right.

When the charge goes from vacuum to medium, the intensity of the transition radiation emitted into the vacuum (backward emission) is easily obtained by changing β to $-\beta$ in formula (9). In the limits $\beta \to 1$ and $|\epsilon| > 1$ the third term of (9) takes the form of a Fresnel reflection term which is not surprising because backward emission comes from those waves which cannot propagate in medium 2 and are reflected from the boundary. As with the forward case, the simplifications of the remaining terms of (9) are applied, yielding the result:

$$\frac{d^2 I_1}{d\omega d\Omega} = \frac{e^2}{\pi^2 c} \left| \frac{\sqrt{\epsilon} - 1}{\sqrt{\epsilon} + 1} \right|^2 \frac{\theta^2}{[\theta^2 + \gamma^{-2}]^2} \qquad (12)$$

Figure 2 shows the strongly peaked angular behavior appearing in both the forward and backward emitted spectral intensities. At lower energy the small-angle intensity is lower,

but still peaks at $\theta \sim 1/\gamma$.

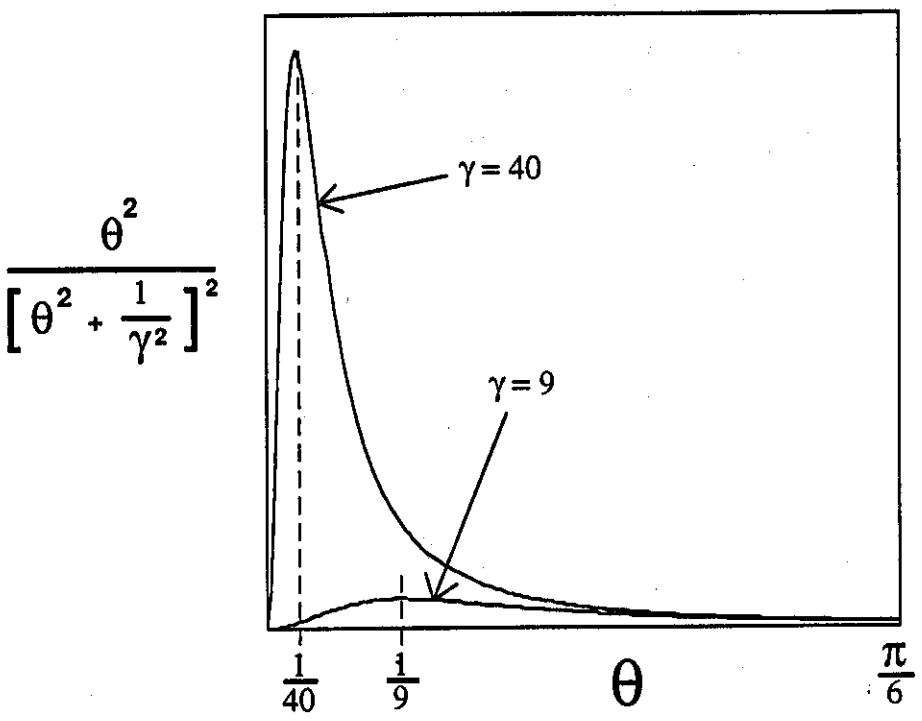

Figure 2. Angular dependence of the spectral intensity per unit solid angle of TR for two different energies...4.5 and 20 MeV.

Equations (11) and (12) are valid whenever relativistic electrons are normally incident on the boundary between vacuum and a medium of dielectric constant ϵ, when $|\epsilon| > 1$. The forms (11) and (12) also correctly reveal the angular behavior when ϵ is close to unity, but slightly less, as is the case for frequencies far above the plasma frequency.

The integration of (11) over θ in the angular interval ($0 \sim \theta_{max}$) gives the energy dependence of the spectral intensity:

$$for\ \theta_{max} < \gamma^{-1} : \quad \frac{dI}{d\omega} = \frac{e^2}{2\pi c}(\gamma\theta_{max})^4 \qquad (13)$$

$$for\ \theta_{max} \sim 1 > \gamma^{-1} : \quad \frac{dI}{d\omega} = \frac{e^2}{\pi c}\left[2\ln(\gamma\theta_{max}) - 1\right] \qquad (14)$$

From (13) and (14), and as can be seen in figure 2, the intensity of TR emitted into very small angles increases with energy as γ^4, while the total intensity has a logarithmic dependence on energy.

Why Metals?

As was shown earlier, for optical frequencies in metals, $|\epsilon| >> 1$. In this case the reflection term in equation (12) tends to unity, and the intensities of forward and backward emission (into the vacuum) are of the same order of magnitude.

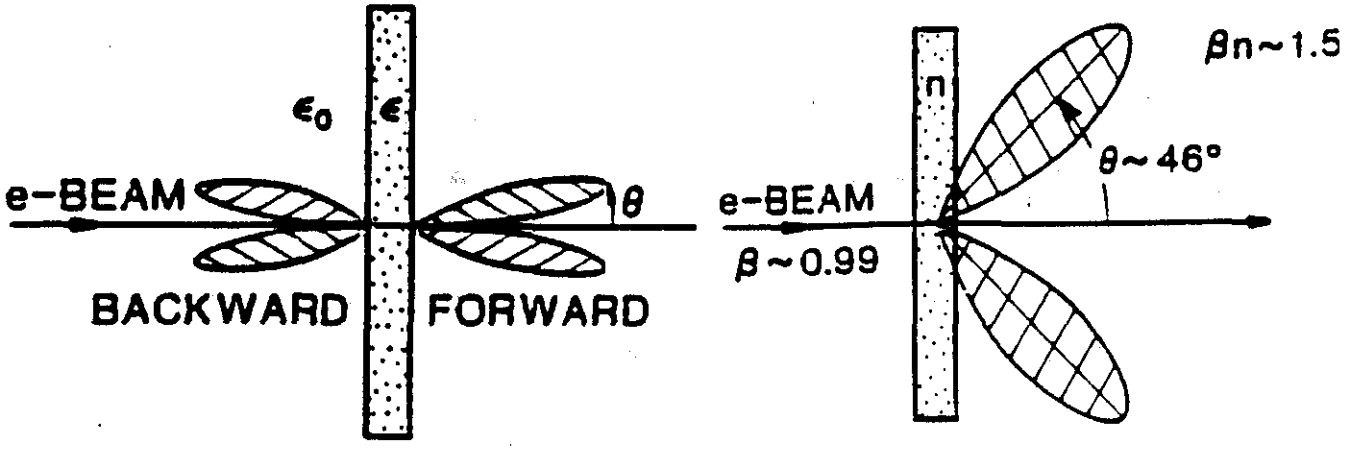

Figure 3. Radiation patterns resulting for the case of normal electron incidence to a metal boundary along with a typical Cerenkov pattern for comparison. These pictures were taken from a paper by Lumpkin *et al.*[11].

Clearly, the radiation pattern emerging from this arrangement is not conducive to non-destructive detection (neither for the beam nor for the detector), because a detector would have to have radiaiton collecting components in the path of the beam. Consider then the case in which the electron is incident on the boundary at an angle of 45°. This is where the importance of a metal boundary comes into play; the radiation emitted as the electron enters the foil (from vacuum) propagates primarily backward as a reflection from the boundary. One might

already expect that the backward emission, resulting from a 45° incidence on a metal, would occur about an axis perpendicular to the electron's direction of motion, as is the case for, say, light reflected from the surface of a mirror.

The general formulae for the case of oblique incidence are rather cumbersome and have been investigated extensively by Pafomov[12]. However, for the case of optical frequencies in metals, the treatment of the problem is greatly simplified by considering the model of a perfectly conducting metallic foil using image charge theory. Transition radiation is then just the radiation emitted in a pair annihilation (or creation) process taking place on the boundary:

$$\frac{d^2I}{d\omega d\Omega} = \frac{1}{4\pi^2 c}\left|\frac{-e\sin\theta}{1-\beta\cos\theta} + \frac{e\sin\theta'}{1-\beta\cos\theta'}\right|^2 \qquad (15)$$

where θ' is the angle of emission with respect to the direction of the image charge velocity (see figure 4).

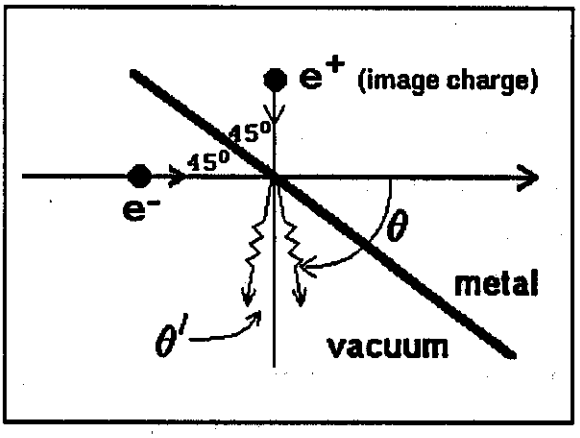

Figure 4. Back radiation for the case of 45° incidence. From equation (1) we know that for relativistic electrons the relevant back emission angle, θ', must be small.

For relativistic electrons ($\beta \to 1$) the first term in equation (15) may be ignored as it tends to unity ($\theta \approx \pi/2$) while the second term blows up (θ' is very small). In this case the back emitted intensity per unit solid angle given by equation (15)

reduces precisely to the form derived in equation (11).

In the medium-to-vacuum case and for relativistic electrons, the second term in (15) may be ignored and the TR is then directed forward into small angles θ with respect to the electron velocity. The forward emission does not strongly depend on the incidence angle, while the backward emission is directed about an axis corresponding to the image charge direction of motion. These assumptions are only valid for the optical range of frequencies emitted from metal boundaries and for non-grazing incidence of electrons with high Lorentz factors. The need for the last condition of large γ can be understood from figure 5, taken from a paper by Wartski et al.[13].

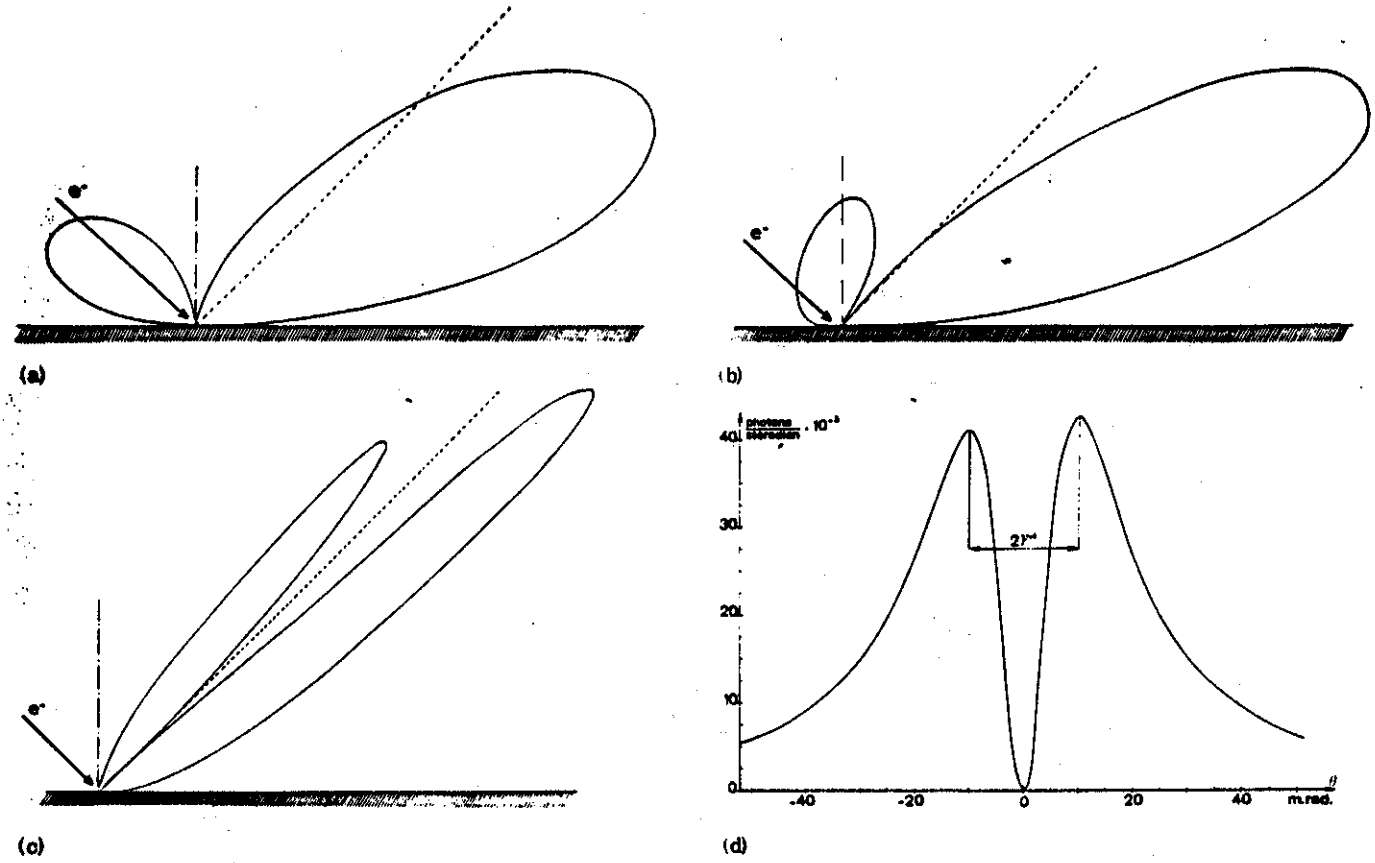

Figure 5. The evolution with γ of the backward OTR (computed from Pafomov's formula) for an electron incident on aluminum at a 45° angle. (a) $\gamma = 1.05$; (b) $\gamma = 2$; (c) $\gamma = 10$; (d) $\gamma = 100$ (not to scale).

When γ is small, the back-emission angles (relative to the axis perpendicular to the electron velocity) are not necessarily small. As γ reaches values on the order of 10 and higher, the backward radiation exhibits the characteristic peaked angular behavior and the asymmetry between the lobes of emitted radiation becomes weak.

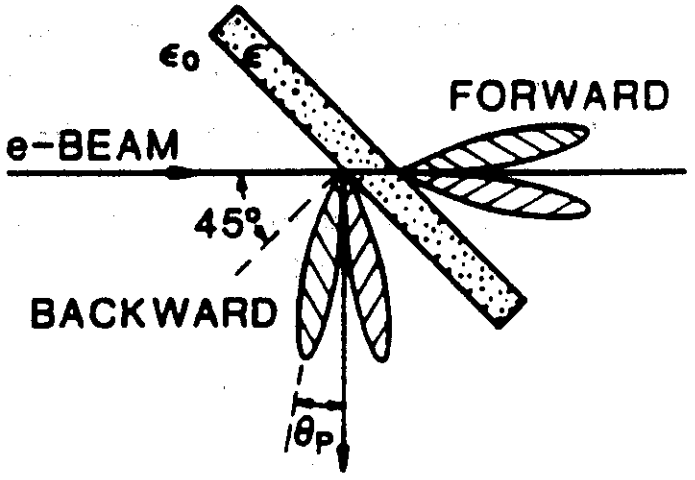

Figure 6. Radiation pattern made by a relativistic electron beam passing through a metal foil at an angle of 45° taken from Lumpkin *et al.*[14].

Hopefully, it is now apparent why this configuration is desired; the back radiation can be easily monitored from a direction perpendicular to the beam axis, without obstructing the beam and making possible the use of cameras and other optical equipment. Also, the image preserves perspective and time structure.

Frequencies Above Optical

The above considerations for metal boundaries were in the limit $\omega < \omega_p$, which includes optical frequencies, where the dielectric constant (6) is negative. As the frequency of radiation rises above the plasma frequency, ϵ becomes positive and the metal no longer reflects the radiation. Note further that at high frequencies, $\omega >> \omega_p$, we have $\epsilon \rightarrow 1$ and in this limit, the back emitted intensity given by equation (12) tends to zero. At high frequencies (in metals and dielectrics) the main part of the energy emitted as transition radiation is in the

forward direction.

It is important to know if there will be harmful radiation (e.g. hard x-rays) emerging from this process. In order to analyze the frequency dependence of the transition radiation, it is necessary to start at equation (2) and retain the relevant dependence on $\epsilon(\omega)$. For high frequencies $\omega >> \omega_p$, again the plasma formula (6) applies and ϵ is very nearly 1. Since in this limit the radiation is mostly forward, the formula for T.R. in the medium-to-vacuum case (equation 9) will suffice to reveal the frequency dependence. With the additional limits: $\beta \rightarrow 1$ and $\theta << 1$, the spectral intensity per unit solid angle takes the form

$$\frac{d^2I}{d\omega d\Omega} = \frac{e^2\theta^2}{\pi^2 c}\left[\frac{1}{1-\beta^2+\theta^2} - \frac{1}{1-\beta^2\epsilon+\theta^2}\right]^2 \qquad (16)$$

Integrating equation (16) over the angles θ, and defining $\omega_{cr} = \gamma\omega_p$ yields:

$$\frac{dI}{d\omega} = \frac{e^2}{\pi c}\left[\left(1+2\frac{\omega^2}{\omega_{cr}^2}\right)\ln\left(1+\frac{\omega_{cr}^2}{\omega^2}\right) - 2\right] \qquad (17)$$

The spectrum of frequencies emitted extends up to the order of ω_{cr}, whereas emission at frequencies $\omega > \omega_{cr}$ is strongly suppressed by a dependence on frequency as ω^{-4}

$$\frac{dI}{d\omega} = \frac{e^2}{6\pi c}\left(\frac{\omega_{cr}}{\omega}\right)^4 \quad \text{limit: } \omega > \omega_{cr} \qquad (18)$$

For the arrangement at UCLA the upper limit $\omega_{cr} \approx 4 \times 10^{17}$ Hz occurs for a 20 MeV beam ($\gamma = 40$) incident on metals $\omega_p \approx 10^{16}$ Hz. The spectral intensity (normalized to optical intensities) in the high frequency limit of the TR spectrum for the UCLA parameters is plotted in figure 7.

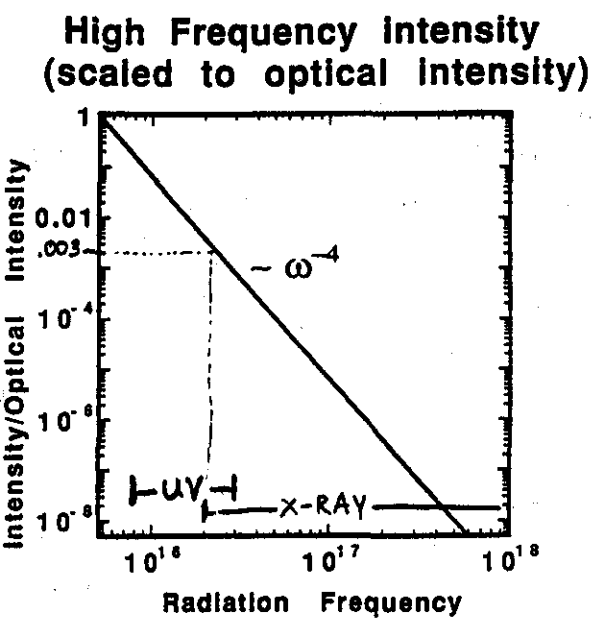

Figure 7. The radiation intensity in the soft x-ray range is already diminished to thousandths of that of the optical range. High frequency TR will not pose a problem for us.

Experimental Considerations

OTR Arrangement and Beam Parameters for UCLA

An initial OTR configuration for the UCLA beam line is shown in figure 8, and the parameters, relevant to OTR, for the UCLA electron beam operating in the single shot mode are given in Table 1.

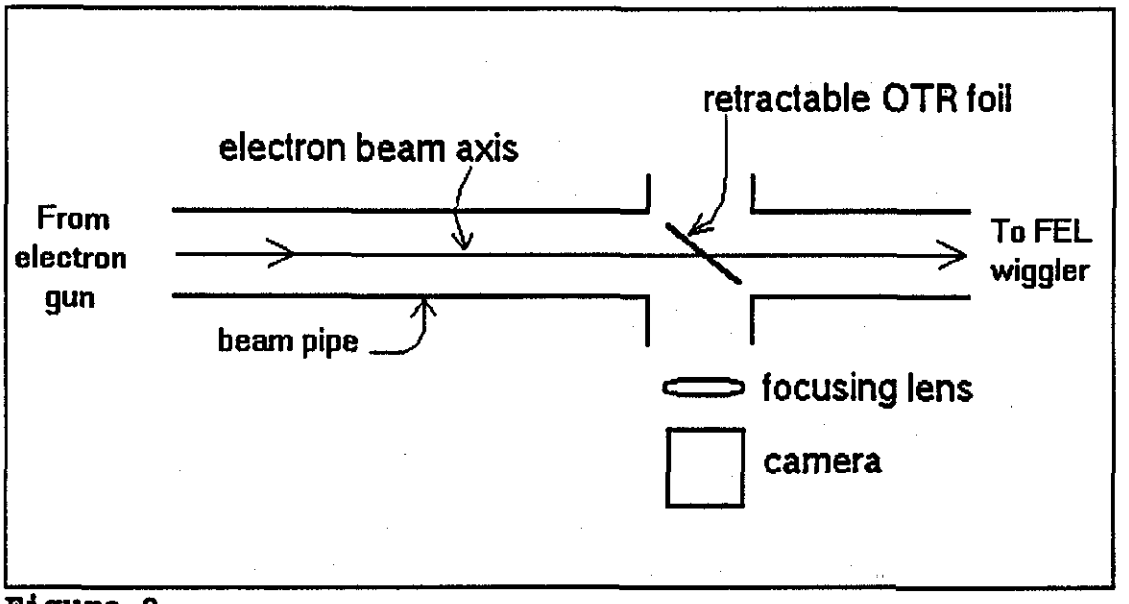

Figure 8

Table 1 Parameters for the UCLA electron beam.

Pulse repetition rate (f_{rep})	5 Hz
Peak current	200 Amp
Bunch length (FWHM)	5 psec
Number of electrons per bunch (N_e)	6×10^9
Typical beam radius (σ_r)	0.25 mm
Cross-sectional beam area ($A_b = 2\pi\sigma_r^2$)	0.39 mm^2
(minimum) OTR target radius (R)	0.5 cm

Yeild of Optical Photons

The choice of optical detector is determined by the number of optical photons emitted. Once these radiometric values are determined they must be compared with the photometric sensitivity of the detector. Consider a typical camera such as the CoHu CCD 4910 series (I chose this one because we have them immediately available to us at UCLA). These cameras are substantially sensitive to light only in the frequency range (2.7 - 4.7) x 10^{15} Hz (see fiugure 9), and have an image area of 6.4 mm x 4.8 mm.

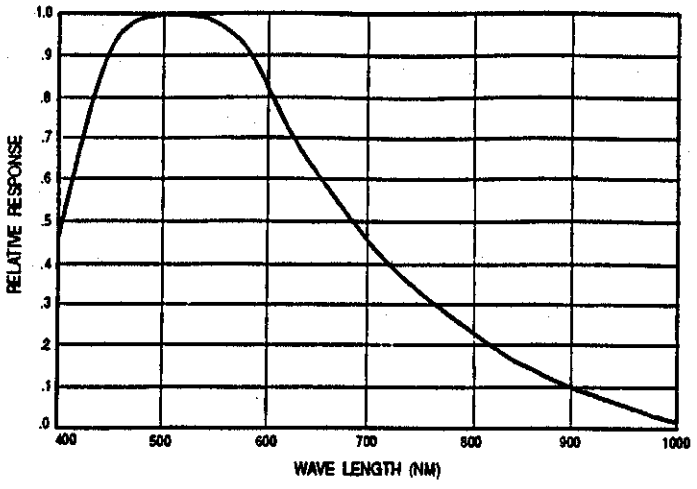

Figure 9. Cohu 4910 sensor spectral response

The luminous sensitivity (photometric units) is rated as follows:

Full video	1.3 lux
80% video	0.1 lux
30% video	0.016 lux

where the 30% video rating is the minimum illuminance that can be imaged by the camera with the gain amplifier fully on.

The number of photons, generated in the frequency interval (ω_1, ω_2) from a single electron incident on a metal foil, is obtained by dividing equation (14) by $\hbar\omega$ and integrating over ω:

$$N = \frac{\alpha}{\pi}\left[2 \ln \gamma - 1\right] \times \ln\left(\frac{\omega_2}{\omega_1}\right) \qquad (19)$$

where α is the fine-structure constant. To obtain the photon yield per pulse equation (19) is multiplied by N_e. For the frequency range of camera sensitivity, the total number of photons per pulse

at 20 MeV is 4.9×10^7,

and at 4.5 MeV is 2.6×10^7.

The conversion of these values to units of lux (= lumens/m^2) is not straightforward; it involves determining the radiant flux, Φ_e(Watts), and scaling this value by an efficacy factor $K(\lambda)$ to find the luminous flux Φ_v(lumens). Then the illuminance (lux) is the luminous flux per unit projected area, A. An approximate determination of these factors done by Rosenzweig[15] yields the following values for use of the CoHu cameras (standard video RS-170 scan time = 1/30 sec.) :

$$\Phi_e = \int \Phi_e(\lambda)d\lambda(\text{visible}) = N(\text{photons}) \times 2.5 \text{ eV} / (\text{scan time})$$

$$K(\lambda) \approx 1/2\ K(\lambda)_{max} = 337 \text{ (lumens/Watts)}$$

Since the resolution (vertical direction) is 350 lines (pixels), the beam spot image area, A, is chosen so that the image size is at least 10 lines tall. (This is not a very good resolution, but

it will allow us to see something.)

$A \sim 1/30$ area of CCD $= 1.02 \times 10^{-6}$ m^2

Finally, the illuminance is given by:

$$\Phi_v/A = K(\lambda)\Phi_e / A \sim N \times 8.2 \times 10^{-9} \text{ lux.}$$

At 20 MeV the illuminance is about 0.2 lux, and at 4.5 MeV it is about 0.1 lux. With the use of the gain amplifier our cameras should be able to view a beam spot by focusing on the foil target. However, in order to observe the angular distribution of OTR the camera must focus at infinity which greatly decreases the illuminance. This makes it necessary to use an intensified camera to image angular distributions.

To give an idea of what the image of an OTR pattern is like, pictures taken from a paper by Maruyama et al.[16] are included. Figure 10(a) showa the angular distribution of OTR produced by an 80 MeV electron beam incident on an aluminized quartz plate at an angle of 45°. Figure 10(b) shows the angular distribution resulting from the same OTR target, but in this case, the beam was first passed through a scattering foil to increase the beam divergence by 1.5 mrad.

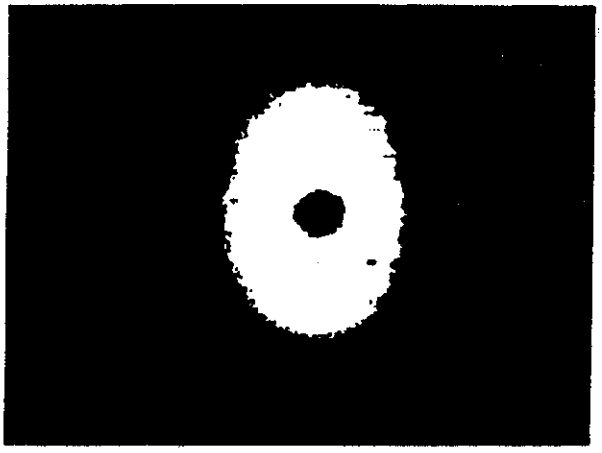

Figure 10(a)

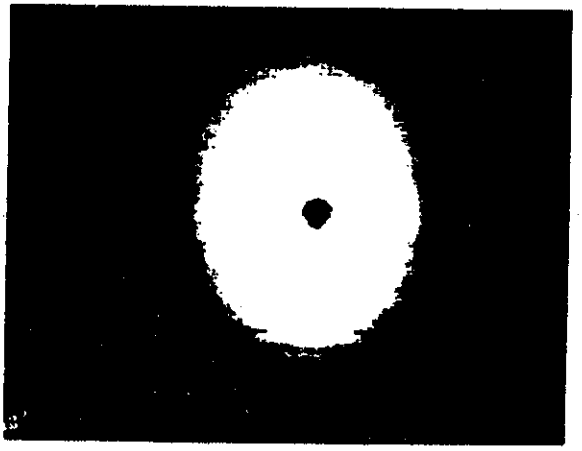

Figure 10(b)

In figure 10(a), the null central intensity is well defined yielding a 'doughnut' shaped pattern. For the increased

divergence case of figure 10(b), the central 'hole' is smaller and the pattern appears more blurred. We see that comparisons of OTR patterns can provide a means of tuning the angular divergence of the beam; in this case differences of angular divergences of only 1.5 mrad can be discriminated with a single OTR foil. A single OTR pattern can be analyzed to measure the angle at which the peak intensity occurs, thus providing a fairly close estimate of the beam energy.

If two foils are used as an OTR interferometer, the beam's energy and divergence can be measured with much greater precision. The basic concepts of this mechanism will be presented at the end of this paper; it is a more involved set-up than a single foil, and requires an intensified camera. At UCLA we will start with one foil, and consider interferometry for the future.

How will OTR affect the beam?

(1) Beam Energy Loss

We must consider the energy lost by the beam upon traversing the target material. There are three principal mechanisms by which the beam looses energy:

(A) Transition Radiation

The energy lost per electron as TR per interface is found by integrating the total spectral intensity, equation (14), over frequencies in the interval $0 - \omega_{cr}$ (the contribution from higher frequencies is small):

$$(dE)_{TR} = I = \frac{e^2 \gamma \omega_p}{\pi c} \left[2 \ln \gamma - 1 \right] \approx \textit{a few eV} \qquad (20)$$

For electrons with energies in the MeV range, this is a negligible energy loss.

(B) Bremsstrahlung Radiation

This is the radiation emitted when moving electrons are slowed by Coulomb collisions with the atomic nuclei of the medium. The energy lost by an electron in traversing a thickness dx of medium is given by Perkins[17](valid for relativistic electrons):

$$\left(\frac{dE}{dx}\right)_{rad} = -\frac{E}{X_0} \qquad (21)$$

Where E is the electron energy and X_0 is the radiation length of the material. The calculated values of this energy loss in 4 different metals are given in table 2.

(C) Ionization of atoms in the target material

In this process moving electrons transfer energy to the material by either ionizing or exciting the atoms there. The energy lost by an electron crossing a thickness dx of medium is given by the Bethe-Bloch formula[18]:

$$\left(\frac{dE}{dx}\right)_{ion} = \frac{4\pi N_A e^4}{mv^2}\frac{Z}{A}\left[\ln\left(\frac{2mv^2}{I(1-\beta^2)}\right) - \beta^2\right] \qquad (22)$$

where m, e, and v are the mass, charge and velocity of the electron, respectively, N_A is Avogadro's number, Z and A are the atomic number and mass number of the atoms in the medium, I is an effective ionization potential (=10Z eV), β = v/c, and x is the path length in the medium measured in g/cm^2. Equation (22) must be multiplied by the mass density, ρ, of the material to obtain a value in units of energy lost per unit distance of material. Numerically, $(dE/dx)_{ion} \approx 1.5$ MeV cm^2/g, and values for 4 different metals and the plastic, Mylar, are given in table 2.

Also, figure 11 shows the behavior of the three energy loss mechanisms at higher energies (up to 10 GeV).

Table 2 Beam Energy Losses (values are per electron)

				4.5 MeV	20 MeV
material	X_o (cm)	ρ (g/cm^3)	$(dE/dx)_i$ (KeV/μm)	$(dE/dx)_r$ (KeV/μm)	$(dE/dx)_r$ (KeV/μm)
Mylar	?	1.5	0.23	?	?
Aluminum	8.85	2.7	0.41	0.05	0.23
Titanium	3.6	4.5	0.68	0.13	0.56
Silver	0.83	10.5	1.58	0.54	2.41
Gold	0.31	19.3	2.9	1.45	6.45

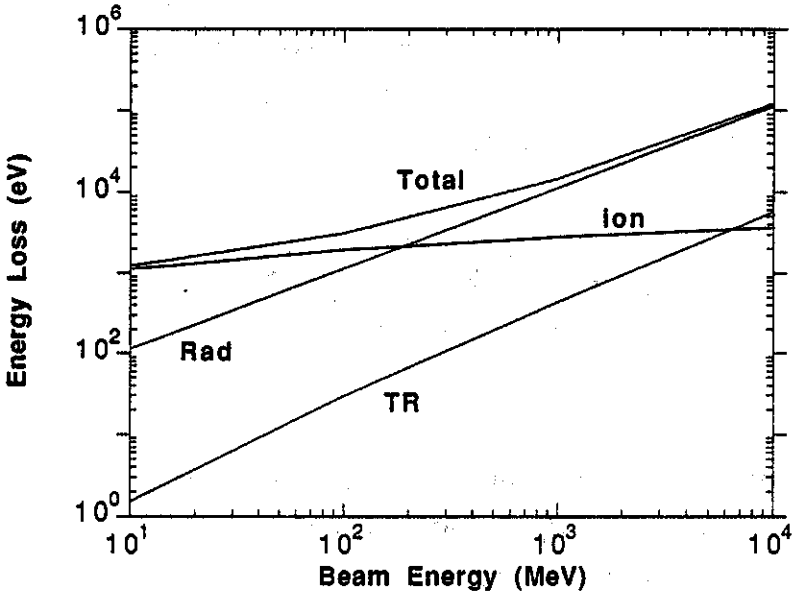

Figure 11. Beam Energy Loss for the range of energies 10 Mev – 10 GeV.

Polyethylene Terephlalates ($C_5H_4O_2$), more commonly known by the commercial name Mylar, is a highly flexible plastic made by DuPont. This substance may be of interest for OTR because it can

be stretched into very thin sheets with smooth reflecting surfaces. Also, extremely thin layers (< 0.5 μm) of any of the metals above (table 2) can be achieved by vacuum deposition of the substances on the surface of Mylar foils (a few μm thick). However, the effects of Mylar on the beam, in terms of Bremsstrahlung radiation and angular divergence (presented next), have to be investigated further, as a value for the radiation length, X_o, is unknown at this time. Another material which has not been investigated is Nitro Cellulose. It is brought to attention by the fact that there are companies which make optical quality sufaces out of the stuff.

The lower limit on thicknesses of pure metal foils used in past experiments, was quoted by Wartski et al.[19] at 0.75 μm for aluminum (manufactured by Goodfellow Co.[20]).

It is clear that for foil thicknesses of a few microns or less, the energy losses per electron are not significant, especially in the lower density materials.

Beam Divergence

Another affect on the beam that is of critical importance to the construction of a non-destructive OTR set-up is the contribution of scattering in the material to the beam's angular divergence. Obviously we want to maintain a low-divergence beam for optimal functioning of the FEL and PWFA systems. The trnsverse dynamics of an electron beam need to be analyzed. Following a treatment by Rosenzweig[21], the horizontal beam size at a some point s along the beam line is given by

$$\sigma_x(s) = \sqrt{\beta_x(s)\ \epsilon_x} \qquad (23)$$

where β_x is a Twiss parameter[22] and ϵ_x is the beam emittance. A similar definition applies for the vertical dimension. The beam

$$\epsilon_{rms,\,x} = \sqrt{\langle x^2\rangle\langle\theta^2\rangle - \langle x\theta\rangle^2} \qquad (24)$$

quality aspect of small beam size is small emittance, ϵ_x, which is defined as the area in phase space occupied by the electron bunch. The rms emittance is defined as:
where the averages (<>) are performed over the beam distribution, and $\theta \equiv dx/ds$. With an rms definition of emittance the rms beam size and inherent beam divergence are, respectively,

$$\sigma_x = \sqrt{\langle x^2 \rangle} \quad and \quad \theta_o = \sqrt{\langle \theta^2 \rangle} \qquad (25)$$

The statistical definition of β_x is therefore $\beta_x = \langle x^2 \rangle / \epsilon_x$, and the value at the beam waist is denoted by the symbol β^*. The rms divergence can be expressed as

$$\theta_o = \sqrt{\langle \theta^2 \rangle} = \sqrt{\frac{\epsilon_x}{\beta^*}} \qquad (26)$$

S. Hartman's simulation[23] of the UCLA gun and linac using PARMELA gives a particle distribution from which ϵ_x and β_x can be calculated. It is convenient to work with the normalized emittance, $\epsilon_{norm} = \beta\gamma\epsilon_x$, which is a constant with $\beta = v/c$ and γ is the Lorentz factor. For the UCLA electron beam,

$$\epsilon_{norm} = 6 \times 10^{-6} \text{ m-rad} \quad \text{and} \quad \beta^* = 0.01 \text{ m}.$$

Thus, the inherent beam divergence has the values:

$$\theta_o(4.5 \text{ MeV}) \approx 8 \text{ mrad}, \quad \text{and} \quad \theta_o(20 \text{ MeV}) \approx 4 \text{ mrad}.$$

Scattering contributions to the beam angular divergence will add in squares to the inherent beam divergence for a Gaussian distribution:

$$\theta_{rms}^2 = \theta_o^2 + \theta_{scat}^2 \qquad (27)$$

The inherent beam divergence actually goes through a range of values as the beam's focus evolves and is controlled by

quadrupole magnets. The positioning of the OTR screen, relative to the beam focus, can be chosen in a way that minimizes the perturbation of the beam.

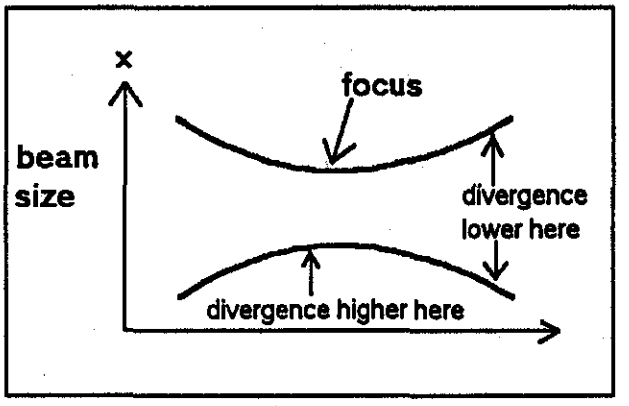

Figure 12. As the electron bunch passes through a focus, the beam size decreases, reaching a minimum at the focus, and then increases with distance from the focus.

The transverse motion of the electrons, and hence the divergence, is high when the beam is being focused down in size. This is the best place for an OTR target to be, because the ratio $\theta_{scatt} / \theta_o$ is a minimum. Whereas, after the focus the electron bunch profile grows larger decreasing the individual transverse motions and the inherent divergence, θ_0. The relative contribution from target scattering to the total rms divergence, θ_{rms}, is thus minimized when the target is traversed on the way to a focus; the total divergence will be closer in value to the inherent divergence, and the perturbation of the beam will be minimized.

As a high-energy charged particle passes through a material, it experiences some scattering from Coulomb interactions with the atoms of the material. For an electron of momentum p, traversing a path length s of material, the rms Coulomb scattering contribution to angular divergence, is given by Perkins[24]:

$$\theta_{scat} = \frac{21}{\sqrt{2}} \frac{1}{p\beta c} \sqrt{\frac{s}{X_o}} \qquad (units\ of\ radians) \qquad (28)$$

where pc is in MeV, $\beta = v/c$, and X_o is the radiation length of the material. Values for different thicknesses of material and

for the two energies relevant at UCLA are given in table 3.

Table 3 Angular divergence from Coulomb scattering

energy→	4.5 MeV		20 MeV	
thickness→	0.5 μm	1 μm	0.5 μm	1 μm
	θ_{scat} (mrad)	θ_{scat} (mrad)	θ_{scat} (mrad)	θ_{scat} (mrad)
Aluminum	7.8	11.1	**1.8**	**2.5**
Titanium	12.3	17.4	**2.8**	**3.9**
Silver	25.6	36.2	5.7	8.1
Gold	41.9	59.3	9.4	13.3

Clearly, at 4.5 MeV we can not hope to preserve a low-divergence beam, however at 20 MeV foils of aluminum or titanium will scatter the beam very little, providing a non-perturbative diagnostic. Note, though, that it is difficult to obtain such thin samples of titanium, so it seems that aluminum, or perhaps aluminum-coated Mylar, is the way to go.

How will the beam affect the target material?

For the first two processes of beam energy loss considered, the energy is radiated away from the target. In the third process, though, the energy lost by the beam is deposited in the target and this will have the effect of heating up the material. Referring to figure 13, the parameter, a, represents an effective radius of the cylindrical volume intercepted by the beam, such that $2\pi\sigma_r^2 = \pi a^2$. L and R are the thickness and radius of the target.

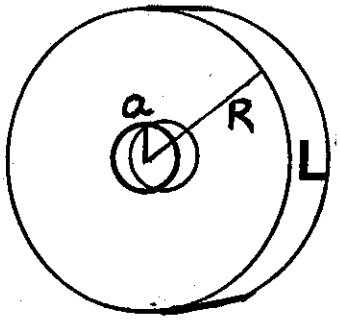

Figure 13. Geometry of OTR target.

The problem of determining the survivability of the material is approached by considering two mechanisms: (1) the heat generated in the target area intercepted by the beam per pulse, (2) the transfer of heat throughout the target with the average current density taken into account. Figure 13 is the relevant geometry for both cases.

(1) Temperature rise of material per pulse

The energy deposited in the material must equal the change in internal energy of the material:

$$\Delta E = \rho c V \Delta T \qquad (29)$$

where ρ and c are the density and specific heat of the material, $V = \pi a^2 L$ is the volume of material into which the energy is deposited, and ΔT is the change in temperature arising in V. In (29) ΔE is the energy deposited by the beam to be found from the Bethe-Bloch equation, (22):

$$\Delta E = N_e (dE/dx)_{ion} \rho L.$$

ΔT is then independent of the parameters ρ and L. Values calculated for the various materials are presented in table 4.

Table 4 Temperature rise of material per pulse

material	c (J / g°K)	ΔT (°K)
Mylar	1.17	0.31
Aluminum	0.897	0.41
Titanium	0.523	0.70
Silver	0.235	1.56
Gold	0.129	2.84

Mylar, Al, and Ti experience only small temperature rises, but we might be wary of Ag and Au targets.

(2) Long term heating

We treat the problem of heat transfer by conduction in a cylindrical system with heat source, q. Since we are dealing with thin targets the temperature dependence along the height of the cylinder may be neglected. The heat transfer equation that must be solved for the temperature, T(r), is:

$$\frac{d^2T}{dr^2} + \frac{1}{r}\frac{dT}{dr} + \frac{q}{k} = 0 \qquad (30)$$

The radius, r, measures the distance from the beam axis in the range 0 - R, k is the thermal conductivity of the material, and the source q is to be determined as the power per unit volume that is generated in the material. The power is just the energy deposited in the material per pulse (from equation (22)) times the frequency of pulse repetition.

$$q = \frac{power}{volume} = \frac{N_o \left(\frac{dE}{dx}\right)_{ion} \rho L f_{rep}}{\pi a^2 L} \qquad (31)$$

The heat is generated only where the beam intersects the target, effectively out to a radius r = a, and q = 0 for r > a. Thus, equation (30) can be solved piece-wise in two regions:

$$\frac{d}{dr}\left(r\frac{dT_1}{dr}\right) = -r\frac{q}{k} \qquad 0 \le r \le a$$
$$\frac{d}{dr}\left(r\frac{dT_2}{dr}\right) = 0 \qquad a \le r \le R \qquad (32)$$

The following boundary conditions are imposed:

$$[1]\ T_1\big|_{r=a} = T_2\big|_{r=a} \qquad [2]\ \frac{dT_1}{dr}\bigg|_{r=a} = \frac{dT_2}{dr}\bigg|_{r=a} \qquad (33)$$
$$[3]\ T_1\big|_{r=0}\ \textit{is finite} \qquad [4]\ T_2\big|_{r=R} = T_{room}$$

Solving for $T_1(r)$ and $T_2(r)$ yields for the temperature change in region 1:

$$\Delta T_1(r) = T_1(r) - T_{room} = \frac{q\,a^2}{4\,k}\left(1 - 2\ln\left(\frac{a}{R}\right) - \frac{r^2}{a^2}\right) \quad (34)$$

and in region 2:

$$\Delta T_2(r) = T_2(r) - T_{room} = \frac{q\,a^2}{2\,k}\ln\left(\frac{R}{r}\right) \quad (35)$$

The temperature rise in the target is greatest at the beam center ($r = 0$); these values are given for various materials in table 5 along with their thermal conductivities, k (Watts / cm°K). The material densities, ρ, are also involved in this calculation, and were presented in table 2.

Table 5. Temperature rise of material (due to 1 nC macropulses at 5 Hz)

material	k (W/cm°K)	ΔT(r=0) (°K)
Mylar	0.003	1.83
Aluminum	2.37	0.004
Titanium	0.22	0.07
Silver	4.27	0.009
Gold	3.15	0.02

Over many pulses the metals have no problem because they conduct the heat appearing in the beam area very quickly to the rest of the target. Mylar has a relatively low specific heat (see table 4), so in a single pulse not much heat is generated in a Mylar target. However, Mylar is a very poor conductor, so over many pulses the heat generated in the beam area is not transferred to the rest of the target as well as in metals. The

full solution, combining equations (34) and (35), is plotted numerically in figure 14(a) with a log scale in 14(b) to include Mylar.

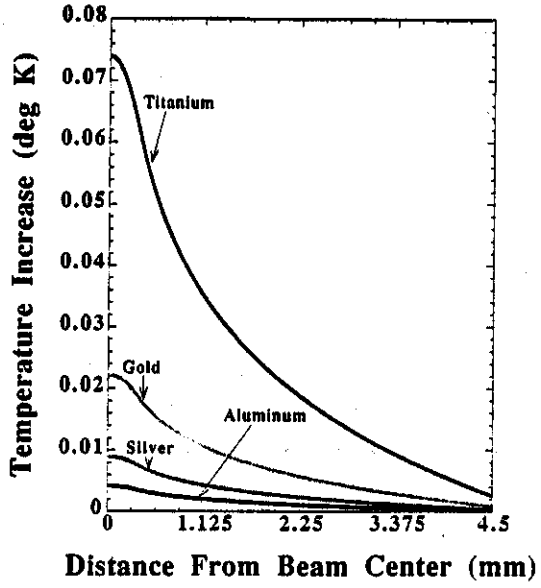

Figure 14(a). Radial dependence of temperature rise in various OTR target foils.

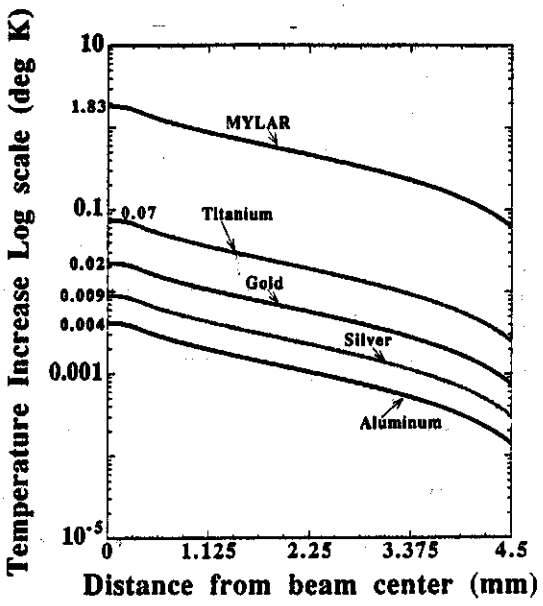

Figure 14(b). Log scale radial dependence of temperature rise in various OTR target foils.

OTR Interferometry

Consider the arrangement of two parallel foils at an angle of 45° to the beam axis. The front face of the second foil acts as a mirror for the forward OTR produced by the first foil. These waves will combine in phase with those of the backward OTR of the second foil since both are produced by the same traversing electron. What results is an interference pattern of radiation centered around the direction of specular reflection. The phase difference between the forward OTR from the first foil and the backward OTR from the second is

$$\phi = (2\pi L/\lambda\beta)(1 - \beta\cos\theta) \qquad (36)$$

where L is the foil separation, and λ is the OTR photon wavelength. The effect is depicted in figure 15, taken from Feldman et al.[25].

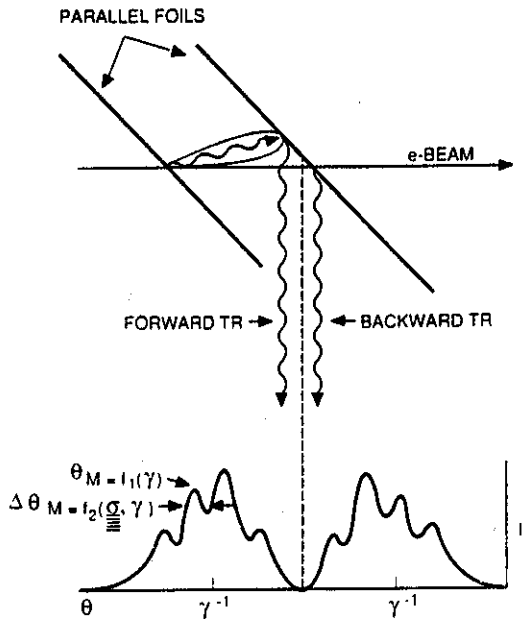

Figure 15. OTR interference and angular dependent spectral intensity patterns.

For relativistic electrons the spectral intensity per unit solid angle of the combined radiation from two interfaces is that

of a single foil multiplied by a Fresnel reflection term $F(\psi,\omega)$ and by an interference term:

$$\frac{d^2I}{d\omega d\Omega} = 4F(\psi,\omega)\,\frac{e^2}{\pi^2 c}\,\frac{\theta^2}{\left[\theta^2+\gamma^{-2}\right]^2}\,\sin^2\left(\frac{\pi L}{2\lambda}\left[\theta^2+\gamma^{-2}\right]^2\right) \qquad (37)$$

where ψ is the incidence angle. The interference order is:

$$p = (L/2\lambda)(\theta^2+\gamma^{-2}) \qquad (38)$$

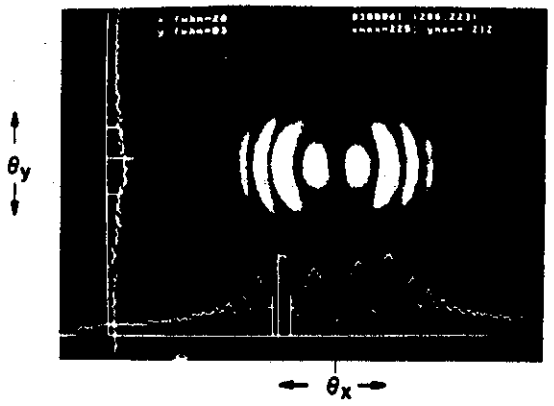

Figure 16. An example of an OTR interferometer image, taken from Lumpkin *et al.*[26].

The intensity minimum correspond to integer values of p, and the maximum to half-integer values. The angular radii of the minima and maxima of the interference fringes is:

$$\theta_{max,\,min} = \left(\frac{2\lambda}{L}\,p-\gamma^{-2}\right)^{\frac{1}{2}} \qquad (39)$$

For each maximum and minimum of the radiation pattern a value of the beam energy can be estimated.

If a Gaussian distribution of beam angles, α, is folded in with equation (37) (or with equation (12)), the spectral intensity per unit solid angle becomes a function of $\theta - \alpha$ multiplied by a normalized Gaussian distribution term[27]:

$$\frac{d^2I(\theta-\alpha,\,\omega)}{d\omega d\Omega} = \int_{-\infty}^{\infty}\frac{d^2I(\theta,\,\omega)}{d\omega d\Omega}\,(2\pi\sigma_r'^2)^{-\frac{1}{2}}\,e^{-\alpha^2/2\sigma_r'^2}\,d\alpha \qquad (40)$$

The integral can be solved analytically to obtain numerical values of the beam characteristics (for use with either single or double foil).

Conclusions

OTR looks promising as an effective non-destructive diagnostic mechanism for the UCLA electron beam that avoids some of the short-comings of methods such as phosphor screens and Cerenkov radiation. Measurements of the beam profile can be obtained with ordinary CCD cameras, and beam energy and divergence may be determined by using intensified cameras to image the OTR angular distribution patterns. Aluminum target foils of a few μm or less are suitable for use. At 20 MeV such targets are predicted to survive long-term beam exposure, while being non-destructive to the beam. At 4.5 MeV, OTR (in any material) will be useful for beam observation, but not in a non-destructive manner. A test OTR arrangement using a mirrored surface quartz plate, inclined at 45° to the beam axis, is already installed for use with the 4.5 MeV beam. OTR interferometry is an appealing future option, because much more information can be extracted from a radiation pattern of many fringes, than from a single doughnut-shaped ring.

Acknowledgements

The author would like to thank James Rosenzweig for guidance towards relevant problems considered in the preliminary calculations for the implementation of OTR, and numerous brief, and insightful, consultations. Also, thanks to Gil Travish for help with organization of ideas, guidance in theoretical development with the utmost of patience, and proof-reading.

References

[1] F. Aghamir et al., Nucl. Inst. and Meth. (1991) NIMO435F.

[2] J.W. Dodd et al.,Intense Laser Beams, Proc. SPIE 1628 (1992)

[3] D.A. Swensen, European Particle Accel. Conf., ed. S. Tazzari, 2 (Rome, Italy, 1988) 1418-20.

[4] M. Hogan, CAA-TECH-NOTE. June, 1992.

[5] V.L Ginzburg and I.M. Frank, Sov. Phys. JETP 16 (1946), 15.

[6] J.D. Jackson, Classical Electrodynamics, Wiley (New York, 1975), 685-6.

[7] M.L Ter-Mikaelian, High-Energy Electromagnetic Processes in Condensed Media, Wiley-Interscience (New York, 1972), 207.

[8] V.L Ginzburg and V.N. Tsytovich, Phys. Rep. 49 (1979) 1.

[9] V.E. Pafomov, Proceedings P.N. Lebedev Physics Institute, ed. by D.V. Skolbel'tsyn, Vol 44 (Consultants Bureau, New York, 1971) 25-157.

[10] J.D. Jackson, ibid, pp. 285-9.

[11] A.H. Lumpkin et al., Nucl. Inst. and Meth. A296 (1990) 151.

[12] V.E. Pafomov, ibid.

[13] L. Wartski et al. J. Appl. Phys. 48 (1975) 3646.

[14] A.H. Lumpkin et al., ibid.

[15] J.B. Rosenzweig, private communication.

[16] X.K. Maruyama, R.B. Fiorito, and D.W. Rule, Nucl. Inst. and Meth. A272 (1988) 238.

[17] D. Perkins, Introduction To High Energy Physics, Addison-Wesley (Reading, Massl, 1982) 43.

[18] D. Perkins, ibid., 39.

[19] L. Wartski et al., ibid. 3648.

[20] Goodfellow Metals Limited, Ruxley Tower, Claygate-Esher, Surrey, England.

[21] J.B. Rosenzweig, private communication.

[22] E. Courant and H.S. Snyder, Ann. Phys. 3 (1958) 1.

[23] S. Hartman, CAA-TECH-NOTE-3/91. February, 1991.

[24] D. Perkins, ibid. 42.

[25] R.B. Feldman, et al., Nucl. Inst. and Meth. A296 (1990)194.

[26] A.H. Lumpkin et al., ibid., 155.